Reactive scattering of Na(32 P 3 / 2)+HCl

M. F. Vernon, H. Schmidt, P. S. Weiss, M. H. Covinsky, and Y. T. Lee

Citation: The Journal of Chemical Physics **84**, 5580 (1986); doi: 10.1063/1.449917
View online: http://dx.doi.org/10.1063/1.449917
View Table of Contents: http://scitation.aip.org/content/aip/journal/jcp/84/10?ver=pdfcov
Published by the AIP Publishing

Reactive scattering of Na(3 $^2P_{3/2}$) + HCl

M. F. Vernon,[a] H. Schmidt,[b] P. S. Weiss, M. H. Covinsky, and Y. T. Lee
Materials and Molecular Research Division, Lawrence Berkeley Laboratory and Department of Chemistry, University of California, Berkeley, California 94720

(Received 5 August 1985; accepted 3 February 1986)

The reaction of electronically excited Na(3*P*) atoms with HCl has been studied in a crossed molecular beams experiment. At collision energies slightly above the endoergicity of the reaction, Na(3*P*) shows a dramatic enhancement of reactivity over ground state Na(3*S*). Detailed measurements of the laboratory angular and velocity distributions of the reactively scattered NaCl product at 5.4 kcal/mol collision energy have allowed determination of the product center-of-mass translational and angular distributions. These experimental results are compared to the DIPR model of electron transfer reactions. The broad translational energy distribution is in qualitative agreement with the DIPR model, but the angular distribution exhibits reduced intensity for scattering perpendicular to the relative velocity vector which cannot be reproduced by the DIPR model. The preferred transition state configuration, Na–Cl–H, is consistent with what would be predicted by a diffuse 3*P* orbital where the Na atom appears ion-like. This configuration is opposite to that given by the dominant term in the long range multipolar expansion of the neutral reactant potential.

INTRODUCTION

The study of reaction dynamics by the crossed molecular beams method has historically been confined to collisions of ground state atoms and molecules. Notable exceptions are metastable states of the rare gas[1] or oxygen atoms.[2] The availability of stable, single frequency tunable dye lasers has recently allowed molecular beam studies involving short lived, electronically excited atoms. A series of papers by Hertel *et al.*[3–6] on the dynamics of collisional quenching of Na*($^2P_{3/2}$) and the works of Zare and co-workers[7–10] on chemiluminescence reactions of Ca(^1P) atoms are pioneering examples.

The current experimental work was undertaken hoping to further our understanding of the dynamics of simple atom–diatomic molecule reactions where one of the reactants, Na(3 $^2P_{3/2}$), is in an excited electronic state. HCl was chosen as a scattering partner because the reaction is 4.68 kcal/mol endothermic in the ground electronic state. This endothermicity allows one to study the interaction between translational and electronic energy in promoting NaCl formation.

The ground state reactions of the alkali-hydrogen halide family have been extensively studied by the molecular beam technique, including the efficiency of vibration, rotation, and translation for promoting reaction.[11–13] Some *ab initio*[14] and semiempirical[15] potential energy surfaces are available and several classical trajectory studies[16] of reactions on these surfaces have been reported. Related theoretical studies of the H + HL mass combination where H and L stand for heavy and light atoms have been published.[17–19] Polanyi[20,21] has reported measurements of the relative reaction cross sections for the Na + HCl (v,J) reaction for $v = 1$–4, $J = 5$–15. The vibrational enhancement indicated gas kinetic reaction cross sections. The dependence of the reaction cross section on the rotational quantum number was rationalized in terms of the preferred HCl–Na orientations for reaction.

In addition to the effect of electronic excitation on the reaction dynamics, the experiments described below can also measure the effect of the alignment and orientation of the Na*($3P_{3/2}$) charge distribution (created by optical pumping of sodium with linearly or circularly polarized laser radiation) on the reactive scattering. The alignment and orientation dependence and the reaction dynamics of higher excited states of Na will be the subject of a future investigation.

EXPERIMENTAL ARRANGEMENT

We have modified our universal, crossed molecular beams machine to allow laser excitation of Na in the collision region in the manner developed by Hertel. Figure 1 shows

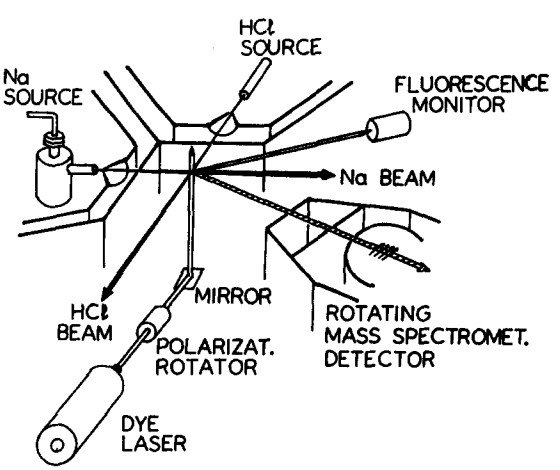

FIG. 1. Schematic diagram of the experimental apparatus showing the orientations of the two molecular beams, mass spectrometer detector, and the laser used for optical pumping.

[a] Present address: Department of Chemistry, Columbia University, New York, New York, 10027.

[b] Permanent address: Freie Universitat Berlin, Fachbereich Physik (FB-20), Institut fur Molekulphysik, 1000 Berlin 33, West Germany.

 0021-9606/86/105580-09$02.10

the experimental topology. Characteristics of the basic apparatus are given elsewhere.[13] Briefly, two supersonic beams are crossed, under single collision conditions, at right angles (beam overlap volume $\sim 10^{-2}$ cm^3) in a liquid nitrogen cooled, 1×10^{-7} Torr vacuum chamber. Scattered product is detected with a mass spectrometer which can rotate in the plane defined by the two reactant beams. The mass spectrometer detector consists of an electron bombardment ionizer, quadrupole mass filter, and a Daly ion counter, enclosed in a triply differentially pumped, ultra-high vacuum chamber.

The sodium atom beam is produced by a rare gas seeded supersonic expansion from a two chamber stainless steel oven. The main oven section, the reservoir for the molten sodium metal, is heated by thermal coaxial heating cable (SEMCO, Inc.) brazed into contact with the oven body. At the top of the reservoir is a stainless steel gas inlet tube affixed onto a miniconflat flange and sealed by a 0.005 in. thick nickel gasket. The gas inlet tube is radiatively heated by a tungsten ribbon. Rare gases, introduced through the inlet tube, enable the average velocity of the sodium atoms to be varied over the range 1.0–3.0×10^5 cm/s at a constant nozzle temperature, here chosen to be 740 °C.

The nozzle chamber consists of a 3.0 in. long, 0.25 in. diameter stainless steel tube, heated by thermal coaxial heating cable brazed into contact with the stainless steel tube. The nozzle aperture is formed by drilling a 0.004–0.006 in. diameter hole in a 0.020 in. thick stainless steel disk, which is welded onto the stainless steel tube. This additional chamber allows the nozzle to be substantially hotter than the reservoir, thus preventing the formation of sodium clusters during the expansion.

The oven chambers are surrounded by two levels of radiation shielding. The temperatures of the reservoir and nozzle are actively stabilized to ± 2 °C of any desired set point. This is necessary to maintain stable intensity and velocity for the sodium beam. Ultra-high purity rare gases, and an all metal, leak tight gas inlet system were found to be necessary to avoid slow clogging of the nozzle.

The central portion of the Na beam is skimmed by a single piece, heated, stainless steel skimmer. The diameter of the skimmer aperture is 0.045 in. diameter and is located 0.25–0.30 in. from the nozzle. The skimmer is also heated by coaxial heating cable.

The dimensions of the sodium beam at the collision region (1 mm tall by 3 mm wide) are determined by a rectangular aperture made from razor blades located in the second differential pumping region. The angular divergence of the Na beam is 1°. Heat radiated from the skimmer is sufficient to prevent clogging of the defining slit from Na condensation.

The HCl beam was formed from a heated stainless steel tube with an interchangeable nozzle affixed on the end. A platinum electron beam aperture (Ted Pella, Inc.) of 70 μ diameter was used in this study. The nozzle temperature was actively stabilized to 180 °C to prevent HCl cluster formation. Typically, 350 Torr HCl nozzle backing pressure was used. A low pressure regulator, in addition to the standard cylinder regulator, was necessary to stabilize the delivery pressure at these low values. A rectangular aperture located in the second differential pumping region defines the transverse HCl beam profile to be 3 mm tall and 3 mm wide at the collision region with an angular divergence of 3°. The HCl velocity distribution was derived from previously measured HCl velocity distributions using the same apparatus but at a higher nozzle temperature (350 °C). The average velocity of the high temperature distribution was multiplied by the ratio of the square root of the two nozzle temperatures to give the average velocity at the lower nozzle temperature. The value obtained, 8.45×10^4 cm/s, is consistent with 99% HCl rotational relaxation in the adiabatic expansion. Unrelaxed, the HCl average velocity would have been 7.23×10^4 cm/s. The full width at half-maximum spread in the HCl velocities was assumed unchanged from the high temperature value of 20%.

The creation of a large, stationary fraction of Na($3\,^2P_{3/2}$) atoms (whose natural lifetime is 16.6 ns) by optical pumping has been exhaustively and elegantly studied by Hertel and co-workers.[22–26] Their experimental technique has been adopted here. Briefly, the selection rule for the change in total angular momentum, $\Delta F = \pm 1$ or 0, ensures that all atoms excited from $^2S_{1/2}(F=2)\rightarrow{}^2P_{3/2}(F=3)$ return to the $^2S_{1/2}(F=2)$ state by spontaneous emission. Thus, the sodium atom behaves as a simple two level system composed of the $^2S_{1/2}(F=2)$ and $^2P_{3/2}(F=3)$ levels when the laser is tuned to this transition.

Several details are pertinent to realizing this maximal excitation efficiency. Power broadening must be less than 60 MHz, the separation of the $^2P_{3/2}(F=2)$ and $^2P_{3/2}(F=3)$ hyperfine (HF) levels. Secondly, the sodium beam angular divergence along the laser beam propagation direction produces an associated transverse Doppler shift. If this Doppler shift is larger than 60 MHz, then some fraction of the sodium beam will be shifted off the $^2P_{3/2}(F=3)$ resonance. For Na seeded in He, this restricts the angular divergence to 1°, the angular spread of the beam in this study.

Even with these precautions there remains uncertainty in the fraction of atoms excited by laser optical pumping to the $3\,^2P_{3/2}(F=3)$ HF level. The small amount of laser energy resonant with the $3\,^2S_{1/2}(F=2)\rightarrow 3\,^2P_{3/2}(F=2)$ transition [even when the laser frequency is locked to the $3\,^2S_{1/2}(F=2)\rightarrow 3\,^2P_{3/2}(F=3)$ transition] can optically pump atoms to the $3\,^2S_{1/2}(F=1)$ ground state. Empirically, in the scattering work of Schmidt and co-workers,[27] a 12% reduction in the inelastic $Na^+ + Na(3S) \rightarrow Na^+ + Na(3P)$ transition was observed when the sodium beam was optically pumped. Unfortunately, in the present Na + HCl scattering experiments, there is no feature in the angular or velocity distributions which can be uniquely assigned to ground state Na($3S$) scattering. If such a feature can be found, its depletion by laser excitation of the Na atoms would measure the effective Na fraction optically pumped to the $3\,^2P_{3/2}$ state. Consequently, in the data analysis below, different values of the excitation efficiency, η, are analyzed. When the conclusions derived are dependent on the assumed value of η, they will be noted.

A combination of commercial camera lenses is used to

image the sodium fluorescence onto a phototube (RCA 1P28) as outlined by Fischer and Hertel.[3] The signal from the phototube, after current amplification (Keithly model 427) drives a lock-in stabilizer (Lansing 80-214) which corrects for frequency drifts. The laser stability is sufficient for greater than 24 h of continuous operation.

Most of the data acquisition is computer controlled. Five basic quantities are measured at each laboratory angle in an angular scan. These are (1) the Na fluorescence intensity (LF), (2) the mass spectrometer signals with the laser on and HCl beam on (L_+X_+), (3) the laser off and HCl beam on (L_-X_+), (4) the laser on and HCl beam off (L_+X_-), and (5) the laser off and HCl beam off (L_-X_-). With the laser off, the difference

$$[(L_-X_+) - (L_-X_-)] \propto \frac{d\sigma}{d\Omega}(3\,^2S_{1/2}) \qquad (1)$$

is proportional to the $3S$ ground state scattering. When the laser is on the mass spectrometer signal will have contributions of a fraction η from $3\,^2P_{3/2}$ scattering and a fraction $(1-\eta)$ from $3\,^2S_{1/2}$ scattering. The following combination of the four mass spectrometer signals is proportional to the $3\,^2P_{3/2}$ differential cross section:

$$\frac{d\sigma}{d\Omega}(3\,^2P_{3/2}) \propto (L_+X_+ - L_+X_-) - (1-\eta)^*(L_-X_+ - L_-X_-). \qquad (2)$$

To obtain the four mass spectrometer data channels, the HCl beam is 100% amplitude modulated by the 150 Hz tuning fork chopper mounted on a water cooled copper block in the HCl beam differential chamber, and the laser beam is 100% amplitude modulated at 3 Hz in phase with the HCl beam modulation by a stepping motor controlled beam stop.

For all data presented, the errors bars for the mean are one standard deviation for the statistical error associated with the finite signal count, or the variance of the mean of the actual measurements, whichever is larger. Typically, four separate angular scans are averaged to obtain approximately 10% error (1σ) in the derived $3P$ distributions. The total counting time at each angle is usually 8 min. The measured quantities at a reference angle are stable within $\pm 1\%$ for the duration of the experiment.

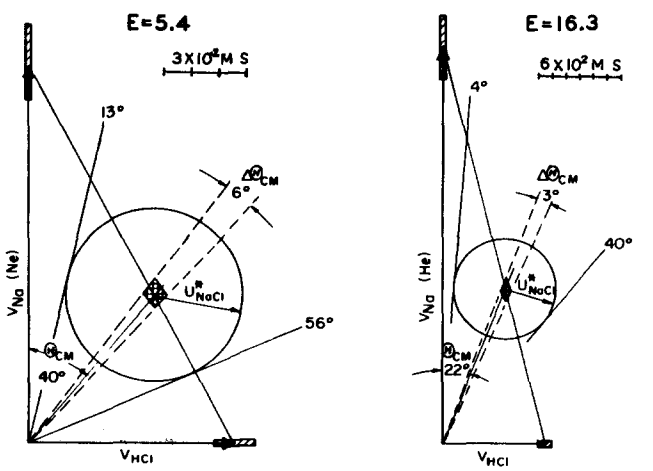

FIG. 2. Newton diagrams for the Na($3P$) + HCl system at the two collision energies, 5.4 and 16.3 kcal/mol, measured in the experiment. The hatched areas show the FWHM velocity distributions at each beam, and the distribution of center-of-mass angles resulting from the reactant beam velocity spreads. The maximal NaCl product velocity is restricted to the circle drawn about the center-of-mass by conservation of energy. The laboratory angles tangent to these circles are the nominal maximum scattering angles for observation of NaCl product.

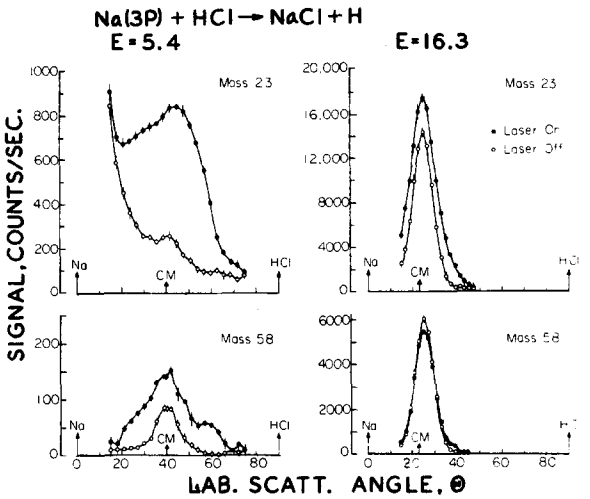

FIG. 3. Na($3S$)/Na($3P$) + HCl scattering angular distributions measured at 5.4 and 16.3 kcal/mol at mass 23 (top) and mass 58 (bottom). The signal is measured in units of the experimentally observed count rates.

Time-of-flight measurements of the product velocity distributions at selected detector angles are obtained by the cross correlation method. The scattered products are correlated to the modulation of the laser by a 255 channel pseudo-random sequence encoded onto a spinning disk placed in the path of the laser beam. Modulation of the laser affects equal densities of the $3S$ and $3P$ sodium atoms because for every Na atom excited to the $3P$ state, one is removed from the ground state. The $3P$ atoms contribute a positive mass spectrometer signal, whereas the $3S$ atoms contribute a negative mass spectrometer signal under laser modulation. The different reactivities of the two electronic states determine the TOF pattern observed. The contributions from the excited state at each laboratory angle, compared to those from ground state, are derived from the angular data by the equation

$$R(\theta) = \frac{d\sigma^*/d\Omega(\theta)}{d\sigma/d\Omega(\theta)} = \frac{(L_+X_+ - L_+X_-) - (1-\eta)(L_-X_+ - L_-X_-)}{\eta(L_-X_+ - L_-X_-)}. \qquad (3)$$

EXPERIMENTAL RESULTS

The Newton diagrams corresponding to the two collision energies, 5.4 and 16.3 kcal/mol, for which data will be presented are shown in Fig. 2. The full widths at half-maximum for the reactant beam velocities, as well as the distribution of center-of–mass angles generated using the average flow velocity of one beam and the half-maximum velocities of the other beam, are shown as hatched areas on the Newton diagrams. The approximate angular broadening caused by

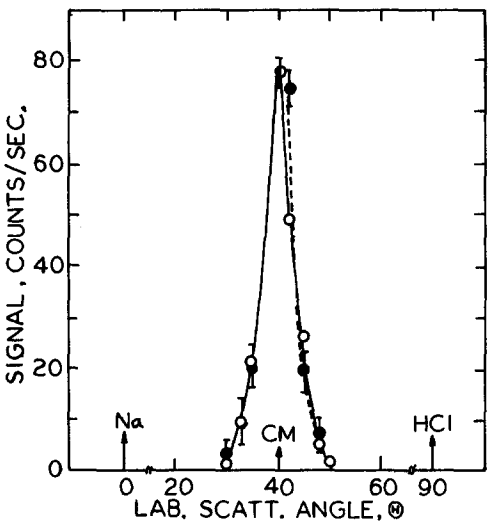

FIG. 4. Calculated (O) and observed (●) NaCl product angular distribution for the Na(3*S*) + HCl reaction at 5.4 kcal/mol collision energy. A constant product translational energy and angular distribution was assumed.

these distributions, $\Delta\theta_{c.m.}$, is also given.

The maximum center-of-mass product velocity allowed in the Na(3*P*) reaction, u^*_{NaCl}, is determined from the reaction endothermicity of 4.68 kcal/mol, the photon energy of 48.43 kcal/mol, and the translational energy corresponding to the average velocity of each beam. The maximum laboratory scattering angles where product can appear from the excited state reaction for the Newton diagram are also indicated.

The angular distributions measured at masses 23 (Na^+) and 58 ($NaCl^+$) with and without laser excitation at two collision energies are shown in Fig. 3. Dramatic enhancement of the reactivity of Na(3*P*) over Na(3*S*) at lower collision energy is evident. As noted above, the reaction Na(3*S*) + HCl→NaCl + H at 5.4 kcal/mol collision energy is slightly above the reaction threshold. For the mass combination of this reaction, and the small amount of energy available for product translational motion, the measured product angular distribution contains no detailed information on the product energy or center-of-mass scattering angle distribution with the current detector resolution and velocity dispersion of the reactant beams. A product flux distribution which is independent of the details of the recoil angular and energy distributions, but consistent with the maximal recoil velocity, reproduces the observed angular variation as shown in Fig. 4.

The mass 23 angular distribution measured at the 5.4 kcal/mol collision energy without laser excitation is predominately elastic or inelastic scattering. A minor reactive contribution is detected at mass 23 near $\theta = 40°$ from fragmentation of NaCl in the electron bombardment ionization process. As the detector sensitivities for mass 23 and mass 58 ions are approximately equal, the fragmentation ratio, $Na^+/NaCl^+$, for NaCl product formed near threshold and ionized by 160 eV can be estimated by subtracting different multiples of the mass 58 purely reactive angular distribution from the mass 23 predominately nonreactive angular distribution. The family of curves generated using multiplicative factors in the range 1–2 is shown in Fig. 5. Assuming negligible depletion of the large angle, nonreactive scattering for this near threshold collision energy, a fragmentation ratio of 50%–55% produces a smooth, monotonic mass 23 angular distribution for the corrected, nonreactive sodium scattering. Variation of the energy of the ionizing electrons in the interval 50–200 V does not markedly change the fragmentation ratio.

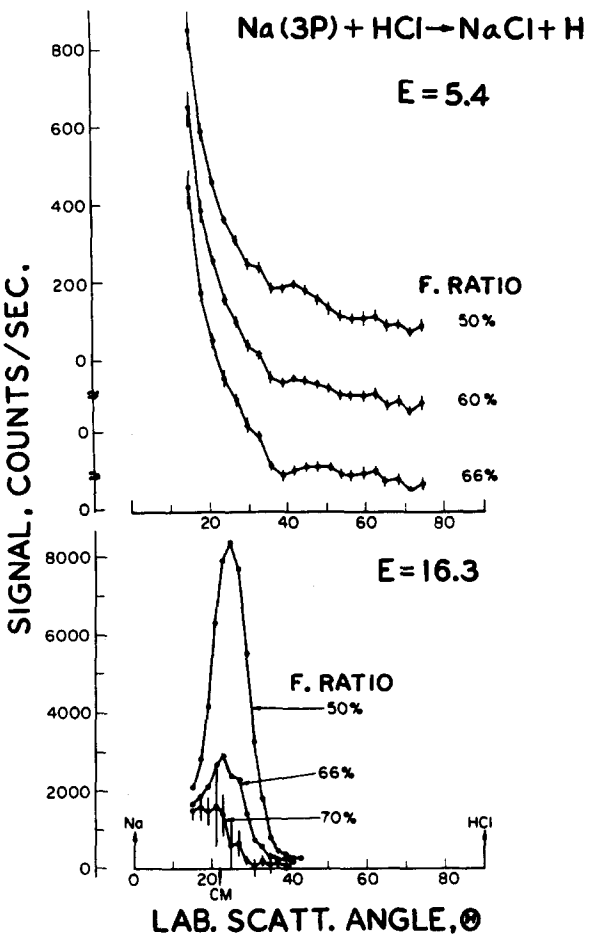

FIG. 5. Mass 23 angular distributions obtained at 5.4 and 16.3 kcal/mol corrected for electron bombardment induced ion fragmentation of the NaCl reaction product assuming different fragmentation ratios.

A similar analysis of the nonreactive Na(3*S*) scattering at the 16.3 kcal/mol collision energy is shown in Fig. 5. At this collision energy, the mass 23 data is dominated by NaCl reaction product ion fragments and correction for the fragmentation is difficult. Unlike the mass 23 angular distribution obtained at a 5.4 kcal/mol collision energy, there is no obvious pure, nonreactive scattering at laboratory angles beyond 15° to enable an interpolation through the angular range dominated by reaction product ion fragmentation. The nonreactive scattering expected to contribute to laboratory angles less than 15° is masked by the effusive Na background from the Na beam source. The best estimate from the 16.3 kcal/mol data gives a fragmentation ratio of near 70%. Fragmentation ratios less than 70% always leave a residual bump near the center-of-mass in the mass 23 angular distribution.

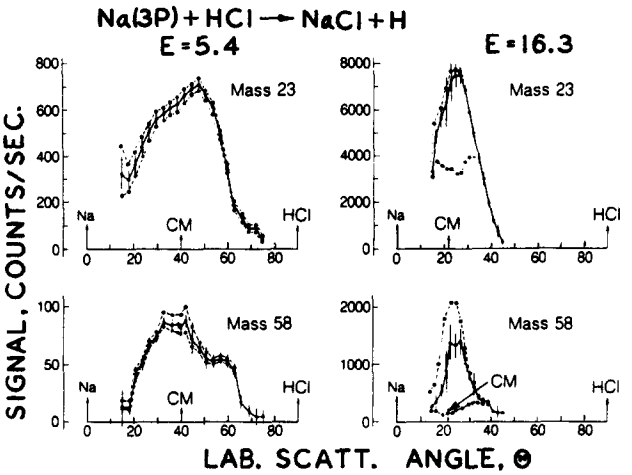

FIG. 6. The derived Na(3*P*) + HCl scattering angular distributions at the two collision energies at mass 23 (top) and mass 58 (bottom) assuming excitation efficiencies of 25% (top curve), 20% (middle curve), and 5% (bottom curve). Error bars are 1 standard deviation of the mean. The signal is in units of the observed count rates.

The mass 23 and 58 angular distributions derived from Eq. (2), assuming different Na*(3*P*) excitation efficiencies for both collision energies are shown in Fig. 6. A 50% error in the fraction of Na atoms assumed to be in the 3*P* state significantly affects the derived Na(3*P*) differential cross sections for the 16.3 kcal/mol collision energy data, while the 5.4 kcal/mol collision energy data are unchanged within the stated measurement errors. For this reason, the 16.3 kcal/mol collision energy data cannot be used to reliably determine center-of-mass differential cross sections.

Laser correlated time-of-flight (TOF) measurements were performed at selected angles for masses 23 and 58 at the 5.4 kcal/mol collision energy. Time-of-flight measurements of the ground electronic state scattering have not been performed. To extract the TOF for the reaction of only Na*(3*P*) atoms from the laser correlated TOFs, the latter were corrected according to Eq. (3) using computed ground state TOF distributions. As stated above, at this near threshold collision energy, the distribution of NaCl product from the ground state reactive scattering is severely convoluted by the distribution of velocity vectors of the center-of-mass of the system. The TOF distributions obtained from the center-of-mass distribution fit to the mass 58 ground state angular distribution are expected to closely approximate the true ground state TOFs. The main effect of correcting the contribution from ground state reaction to the TOF's using Eq. (3) is to boost the signal at 35°, 40°, and 45° for the channels near the center-of-mass slightly. As the 3*P* state is approximately ten times more reactive than the 3*S* state, the corrected channels are displaced within their original 1σ statistical error. The corrected mass 23 TOF data are shown in Fig. 7. The TOF data at the laboratory angles 25° amd 30° clearly exhibit a fast, Na(3*P*) elastic peak as well as a slower, broader, reactive ion fragment peak.

In general, the error in the assumed fraction of Na(3*P*) atoms in the collision volume can have a dramatic effect on the extraction of the TOF distribution for Na*(3*P*) scattering from the laser correlated TOF data. The relative weight-

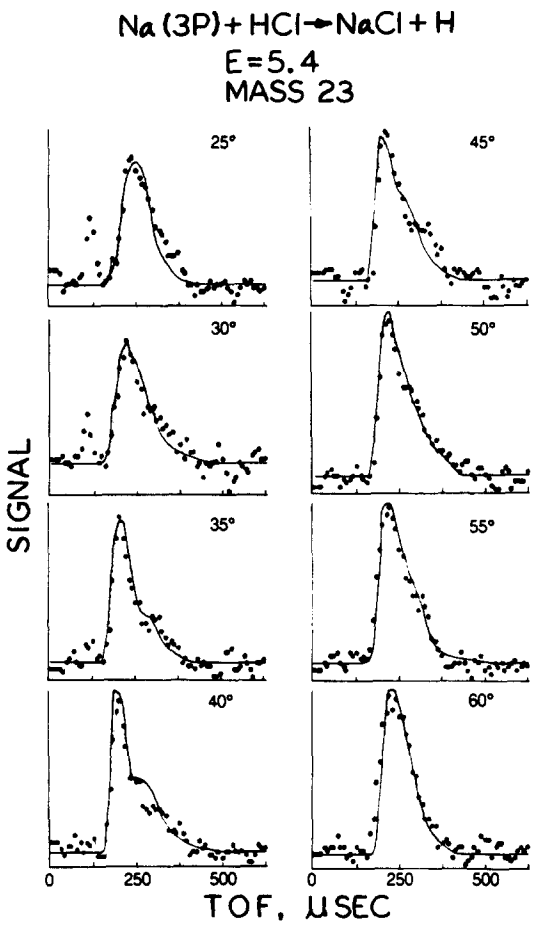

FIG. 7. Experimental laser correlated time-of-flight distributions at mass 23 for the collision energy of 5.4 kcal/mol for the indicated laboratory angles. At 25° and 30°, elastic scattering of Na(3*P*) atoms can be easily seen. The slow, broader peak at all angles is assigned to NaCl product which fragments in the electron impact ionizer for Na^+. The solid line is the fit to the data given by the numerically determined center-of-mass scattering distribution.

ing of the Na(3*S*) TOF to the laser correlated TOF depends on the ratio of the contribution of Na(3*P*) to Na(3*S*) atoms at that laboratory angle. In turn, this depends on what fraction of the Na atoms we assume to be Na*(3*P*). At the collision energy 5.4 kcal/mol, the laser induced signal is large compared to the ground state scattering signal. Large errors in the fraction of Na atoms excited does not significantly affect the derived center-of-mass energy and angular distributions of products. For the 16.3 kcal/mol collision energy, the ground state signal is comparable to the laser induced signal and the assumed value for the Na(3*P*) fraction can qualitatively affect the shape of the angular and TOF data used to obtain the center-of-mass product flux distributions.

DATA ANALYSIS

The angular and velocity distributions measured at masses 23 and 58 in the scattering of Na(3*P*) + HCl can have contributions from the following collision processes:

Reaction

$$Na(3P) + HCl(v = 0) \rightarrow NaCl + H(^2S), \quad (4)$$

$$Na(3P) + HCl(v = 0) \rightarrow NaH + Cl(^2P_{3/2}), \quad (5)$$

Quenching

$$Na(3P) + HCl(v=0) \rightarrow Na(3S) + HCl(v',J'), \quad (6)$$

Elastic or rotational inelastic

$$Na(3P) + HCl(v=0) \rightarrow Na(3P) + HCl(J'). \quad (7)$$

Analogous to the Na($3S$) reactive scattering, NaCl product is expected to be favored over NaH. Significant contributions from quenching can be ruled out for kinematic reasons. The fast TOF peak observed at small angles can be easily assigned to elastic scattering because its position is exactly predicted by our reactant beam velocities and because it is absent from the mass 58 velocity distributions. If the slow product were caused by quenching of Na($3P$), then the internal energy of the scattered HCl must be *greater than* 55 kcal/mol and less than 58 kcal/mol. To our knowledge, this specificity of energy disposal has never been observed in the Na($3P$) quenching studies of Hertel *et al.*[3–6]

Secondly, the angular distributions measured at 16.3 kcal/mol collision energy imply even greater energy retention by the diatomic product than at lower collision energy if quenching was the dominant collision process. However, assigning all of the slow, Na^+ TOF data to NaCl ion fragments is not only consistent with the kinematic and energetic constraints of this channel, but also logical since angular distributions of scattered products measured at mass 23 are similar to those measured at mass 58 ($NaCl^+$).

Unlike the ground electronic state scattering, the contribution to the mass 23 angular distribution originating from NaCl product cannot be quantitatively predicted from the corresponding mass 58 distributions (see Fig. 6). The difference in the shape of the two angular distributions is due to the internal energy dependence of the NaCl ion fragmentation ratio. From the ground state Na($3S$) reactive scattering analysis, it was noted that at threshold and 12 kcal/mol above threshold, the NaCl fragmentation ratio changed from 50% to 70%. For the Na($3P$) angular distributions, this ratio is not observed. The $NaCl^+$ signal is only 1/10 of the mass 23 signal at the peak of the 5.4 kcal/mol angular distribution. Since the vibrationally/rotationally excited NaCl produced in the Na($3P$) reaction fragments under electron bombardment ionization, the mass 23 angular distribution is a more accurate measure of the true NaCl reactive product angular distribution. For example, a change in the fragmentation ratio from 90% to 92% for $NaCl^+$ will affect the mass 23 distribution by 2% while changing the mass 58 distribution by 20%. Of course, allowance for Na($3P$) elastic scattering must be done at small angles.

The most accurate procedure would be to sum the TOF distributions for the daughter and parent ions of NaCl. When this is done, it is found that the relative change in the shape of the mass 23 distributions is within the statistical error of the original mass 23 data.

Center-of-mass NaCl product flux distributions were derived from the experimental data using a computer program. The computer program accounts for the kinematic averaging caused by the distribution of reactant beam velocities and the finite spatial and temporal resolution of the detector. The program generates time-of-flight and angular distributions corresponding to an input center-of-mass distribution, which are then directly compared to the laboratory measurements. By trial and error, a center-of-mass distribution which best represents the measurements is found.

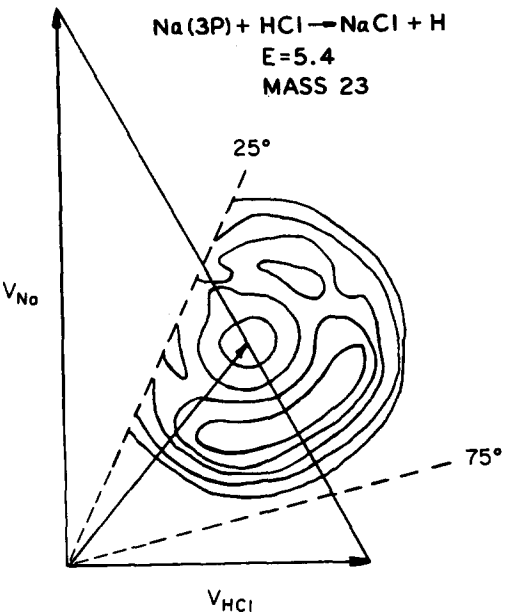

FIG. 8. Optimal center-of-mass NaCl product flux distribution determined from the analysis of the TOF and angular data for the 5.4 kcal/mol collision energy.

In the analysis of the 5.4 kcal/mol data the total reaction cross section was considered independent of the collision energy. The range of collision energies is sufficiently narrow in the experiment so this assumption should not introduce significant error, except near threshold where the reaction cross section might have a strong translational energy dependence.

For finding the best fit center-of-mass distributions, a numerical table specifying the probability of scattering at selected center-of-mass recoil velocities was found useful. The scattering angles and recoil speeds representing the table entries were distributed over the range of the observed product with a sampling density guided by the kinematic averaging induced by the spread of reactant velocities.

The best center-of-mass flux distribution is shown in Fig. 8 and compared to the experimental data in Fig. 7. Essentially exact agreement with the experimental data can be obtained if unrestricted variation of a sufficiently dense grid of the table entries is allowed. The resulting distribution is symptomatic of high parameter correlation and not uniquely determined by the data. The best fit distribution is a subjective compromise between faithful reproduction of the experimental data and meaningful parameter extraction. The energy averaged center-of-mass recoil angle distribution and the recoil angle averaged, center-of-mass energy distribution are given in Fig. 9 for the best fit distribution.

DISCUSSION

The Na*($3P$) + HCl reaction has some of the expected features of a prototypical electron transfer reaction. The essence of this model is that during an early phase of the reaction, an ionic complex is formed by transfer of the Na($3P$)

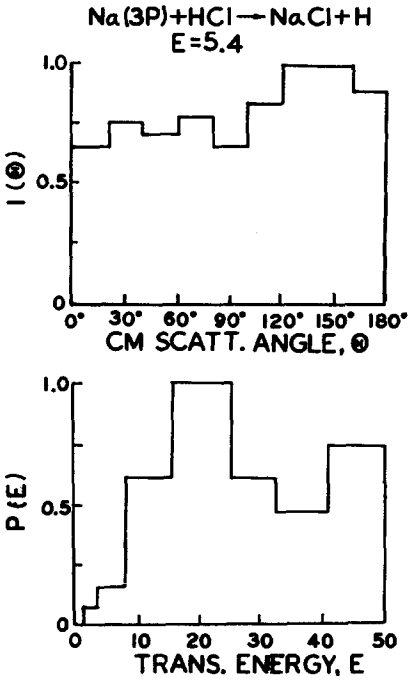

FIG. 9. Translational energy averaged product angular distribution and scattering angle averaged translational energy distribution for the best fit center-of-mass scattering distribution for the 5.4 kcal/mol collision energy.

electron to HCl. If the electron transfer occurs rapidly compared to the nuclear motion, HCl^- should be formed with a distribution of internuclear separations given by a vertical projection of the HCl vibrational wave function onto a dissociative, repulsive region of the HCl^- potential. Due to the light mass of the H atom, if H does not interact strongly with Na^+, it should quickly separate from the Na^+/Cl^- ion pair which subsequently associated into a NaCl molecule under the influence of attractive Coulombic forces. A solvable, classical model for this type of reaction is the DIPR (direct interaction with product repulsion) model originated by Polanyi[28] and elaborated by Herschbach and co-workers.[29] Rettner and Zare[30] have recently extended and applied this model to chemiluminescent reactions.

The DIPR model is expected to be accurate for A + B-C→AB + C reactions which proceed first by release of the BC^- repulsive energy subsequently followed by A^+B^- attraction. Secondly, A^+ should interact weakly with the B^- and C atoms while BC^- dissociates, and similarly for C with A^+ and B^- while the latter pair associates. Clearly, a steep and repulsive BC^- potential with large exothermicity will favor a short time scale for the release of the repulsive energy. In the Na + HCl reaction, the mass combination favors a rapid departure of the H atom. Using theoretical potential curves for HCl and HCl^-,[31] the Frank–Condon region accessible from the ground vibrational state of HCl predicts product translational energies in the range 10–40 kcal/mol. This compares favorably with the range observed in the experiment.

From the above discussion, it would appear that the Na*(3*P*) + HCl reaction would be an ideal candidate for the DIPR model. However, the DIPR model is based on the electron transfer occuring at relatively large reagent separation where the repulsive energy release occurs prior to product bond formation. The intermolecular distance where the electron transfer takes place is, to first order, calculated from the − 23 kcal/mol vertical electron affinity of HCl($v = 0$)[31] and the + 76 kcal/mol ionization potential of Na(^3P). These values predict that the electron will transfer to HCl when the Na*(3*P*)–HCl separation is ~3.5 Å. However, the outer peak of the electron probability distribution for Na(3*P*) extends from 3–4 Å, with a maximum at 3.5 Å. This means that the electron jump occurs when the HCl molecule has penetrated the 3*P* orbital of Na*(3*P*). The close proximity of the Na^+ ion may invalidate applying the DIPR model in this case. Instead of two distinct reaction phases characterized by sequential two-body interactions, the reaction might be more accurately viewed as a process in which the initial electron transfer is followed by repulsive energy release between the H atom and the Na^+Cl^- molecule as a whole.

The total reaction cross section is expected to be affected in approximately the same way by either Na electronic energy or HCl vibrational energy if the electron transfer were to play an important role. This is because the vibrational excitation increases the HCl electron affinity while the electronic excitation reduces the Na ionization potential. To first order, the reaction cross section will depend only on the energy difference between the Na ionization potential and the HCl electron affinity. Consequently, the enhancement of the reaction cross section for Na(3*P*) or vibrationally excited HCl,[20,21] is consistent with the electron transfer model.

The center-of-mass product distribution is a good test of the applicability of the DIPR model. To apply the model we need to specify the distribution of product velocities. Within the DIP approximation,[29] this would be given by projecting the HCl($v = 0$) nuclear wave function onto the HCl^- potential. Since we do not know the distribution of HCl bond lengths when the electron jumps, we extract an optimal translational energy distribution from the experimental data as done above only now the kinematic relation of the DIPR model must be satisfied.

For example, the DIPR model relates the center-of-mass scattering angle, X, the initial and final translational energies, E_i and E_f, to the ratio of the momentum change to the initial momentum, q, via Eq. (8):

$$q^2 = \left(\frac{100E_f}{E_i} + 1\right) - 2|\cos X|\sqrt{\frac{100E_f}{E_i}}. \tag{8}$$

Once q is known, the angle ρ which the diatomic must have with respect to the relative velocity vector at the transition state is given by Eq. (9):

$$\cos\rho = \frac{1}{|q|}[\sin^2 X - \cos X(q^2 - \sin^2 X)^{1/2}]. \tag{9}$$

If there are preferred configurations for the transition state, then these will show up in the X, E_f dependence of the center-of-mass scattering distributions through Eqs. (8) and (9). We parametrize the orientational preference for $\cos\rho$ by a simple function suggested by Marron[32]:

$$T(\rho) = (1 + \cos\rho)^n. \tag{10}$$

In summary, the parameter n and the histogram representa-

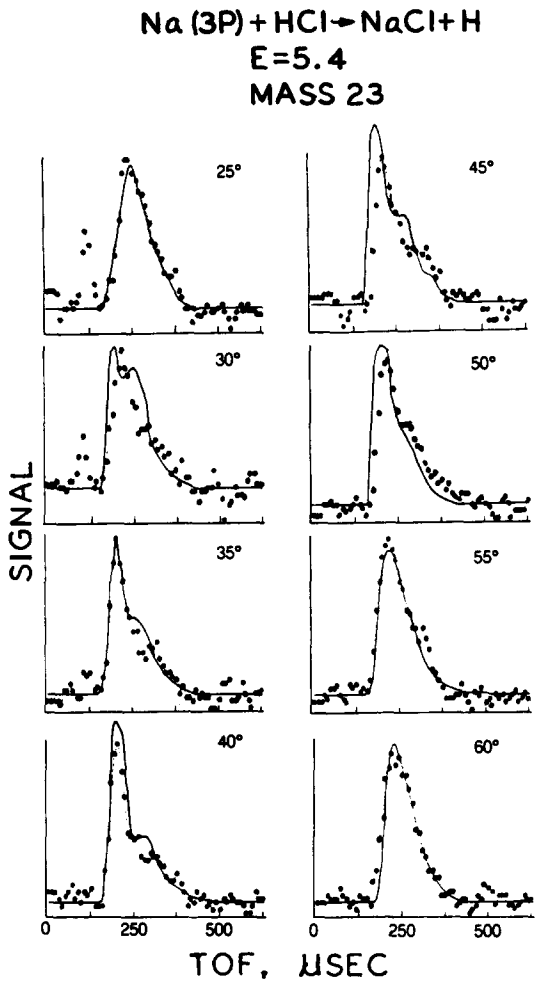

FIG. 10. Best DIPR model fit to the experimental TOF data for the collision energy 5.4 kcal/mol.

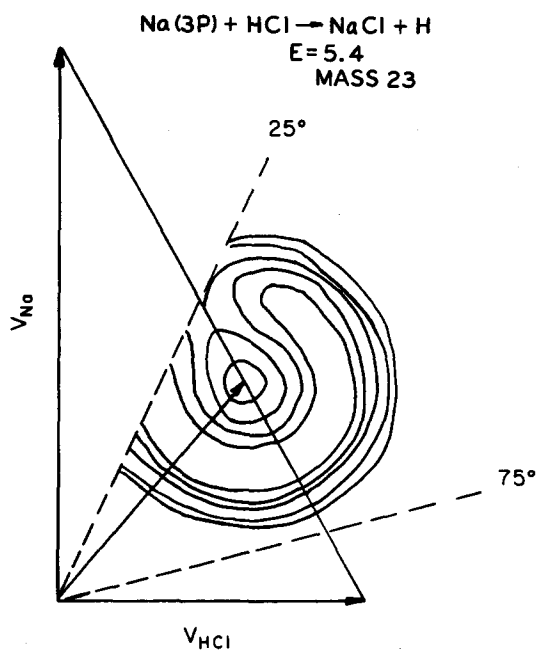

FIG. 11. Best DIPR model fit center-of-mass product flux distribution for the collision energy 5.4 kcal/mol.

tion of E_f are varied to find a best fit to the measured TOF and angular data.

In Figs. 10 and 11 we show the best fits obtained using the DIPR model. Comparison of the DIPR model fit with the best fit coupled center-of-mass distributions shows the largest difference for scattering perpendicular to the relative velocity vector. In the DIPR model, it is not possible to have a reduced intensity along this scattering angle. However, the anisotropy parameter n is small ($n \sim 0.24 \pm 0.07$) indicating that there is nearly an isotropic distribution for the HCl at the moment of the electron jump. The extracted reaction anisotropy favors the Na–Cl–H configuration. This is in accord with the predicted configuration if the valence electron is diffuse, i.e., $Na^+ + Cl$–H and not that of the dominant long range multipole interaction (quadrupole–dipole) which would favor Na–H–Cl. The translational energy distribution for the DIPR model fit is broad, with almost equal probability from 10–50 kcal/mol. This covers the predicted energy range of the DIPR-DIP model using the isolated HCl^- potential curve discussed previously.

Finally, if the DIPR model is qualitatively correct for the reaction of Na($3P_{3/2}$) + HCl, higher energy Na electronic states should have nearly the same product translational energy, as this is primarily determined by the H–Cl^- repulsion after electron transfer. The additional electronic energy should appear as vibrational excitation of NaCl. The higher excited electronic states have a larger electron jump distance, and since the H atom will depart rapidly, the conversion of the potential energy of the Na^+–Cl^- ion pair at the electron jump distance to product translational energy will be small. On the other hand, if the repulsive energy release cannot be adequately described solely by the H–Cl^- repulsion and the extent of NaCl bond formation or electronic symmetry has to be considered, then the translational energy distributions of products will depend on the electron jump distance and the level of electronic excitation. This question will be pursued in the future.

CONCLUSIONS

The results of a crossed molecular beam study of the Na($3\,^2P_{3/2}$) + HCl reaction have been compared with a sequential two-body model (the DIPR model) which is known to successfully explain reactions characterized by long range electron transfer. Qualitatively, the experimental scattering is similar to what the DIPR model would predict using only theoretical data available from the literature. The differences between the observed scattering distributions and those which can be generated by optimizing the parameters of the DIPR model were concluded to originate from a breakdown in the assumption of sequential release of repulsive and attractive energy. This is consistent with the small internuclear distance of the electron transfer, which imparts a degree of "concertedness" to the reaction. Future experiments on the reactions of higher electronic states of sodium will provide an interesting comparison on the validity of a two body sequential model.

ACKNOWLEDGMENTS

This work was supported by the Director, Office of Energy Research, Office of Basic Energy Sciences, Chemical

Sciences Division of the U. S. Department of Energy under Contract No. DE-AC03-76SF00098. H. S. wishes to thank the Deutsche Forschungsgemeinschaft for financial support.

[1]R. Hennessy, Y. Ono, and J. P. Simons, Mol. Phys. **43**, 181 (1981).
[2]R. Buss, P. Casavecchia, T. Hirooka, S. Sibener, and Y. T. Lee, Chem. Phys. Lett. **82**, 386 (1981).
[3]A. Fischer and I. Hertel, Z. Phys. A **304**, 103 (1982).
[4]I. Hertel and W. Stoll, J. Appl. Phys. **47**, 214 (1976).
[5]I. Hertel and W. Stoll, Adv. At. Mol. Phys. **13**, 113 (1978).
[6]H. Hermann and I. Hertel, Comments At. Mol. Phys. **12**, 61, 85 (1982).
[7]M. Prisant, C. Rettner, and R. Zare, Chem. Phys. Lett. **88**, 271 (1982).
[8]M. Prisant, C. Rettner, and R. Zare, J. Chem. Phys. **75**, 2222 (1981).
[9]C. Rettner and R. Zare, J. Chem. Phys. **75**, 3636 (1981).
[10]C. Rettner and R. Zare, J. Chem. Phys. **77**, 2416 (1982).
[11]F. Heismann and H. Loesch, Chem. Phys. **64**, 43 (1982).
[12]M. Hoffmeister, L. Potthast, and H. J. Loesch, Chem. Phys. **78**, 369 (1983).
[13]C. Becker, P. Casavecchia, P. Tiedemann, J. Valentini, and Y. T. Lee, J. Chem. Phys. **73**, 2833 (1980).
[14]M. Chen and H. F. Schaefer, J. Chem. Phys. **72**, 4376 (1980).
[15]M. Shapiro and Y. Zeiri, J. Chem. Phys. **70**, 5264 (1979).
[16]I. Noorbatcha and N. Sathyamurthy, Chem. Phys. **77**, 67 (1983), and references therein.
[17]N. Hijazi and J. Polanyi, Chem. Phys. **11**, 1 (1975).
[18]K. Schulten and R. G. Gordon, J. Chem. Phys. **64**, 2918 (1976).
[19]H. Baer, Mol. Phys. **26**, 369 (1973).
[20]F. Bartoszek, B. Blackwell, J. Polanyi, and J. Sloan, J. Chem. Phys. **74**, 3400 (1981), and references therein.
[21]B. Blackwell, J. C. Polanyi, and J. C. Sloan, Chem. Phys. **30**, 299 (1978).
[22]N. Reiland, C. Schulz, H. -V. Tittes, and I. Hertel, Chem. Phys. Lett. **91**, 329 (1982).
[23]W. Reiland, G. Jamieson, H. -V. Tittes, and I. Hertel, Z. Phys. A **307**, 51 (1982).
[24]W. Reiland, H. Tittes, I. Hertel, V. Bonacic-Koufecky, and M. Persico, J. Chem. Phys. **77**, 1908 (1982).
[25]P. Botschwina, W. Meyer, I. Hertel, and W. Reiland, J. Chem. Phys. **75**, 5438 (1981).
[26]W. Reiland, H. Tittes, and I. Hertel, Phys. Rev. Lett. **48**, 1389 (1982).
[27]H. Schmidt, A. Bahring, E. Meyer, and B. Miller, Phys. Rev. Lett. **48**, 1008 (1982).
[28]P. J. Kuntz, M. H. Mok, and J. C. Polanyi, J. Chem. Phys. **50**, 4623 (1969).
[29]D. P. Herschbach, Discuss. Faraday. Soc. **55**, 233 (1973).
[30]M. G. Prisant, C. T. Rettner, and R. N. Zare, J. Chem. Phys. **81**, 2699 (1984).
[31]J. N. Bardsley and J. M. Wadehra, J. Chem. Phys. **78**, 7227 (1983).
[32]M. Marron, J. Chem. Phys. **58**, 153 (1973).